TEM IMAGING TECHNIQUE①

He, Jishan Ren, Baolin
Centcal South University of Technology, Changsha 410083, China.

ABSTRACT

This imaging technique is used for approximate interpretation of TEM data including ungrounded loop source and grounded line source soundings. Loop source data can be collected as central-loop soundings or as out-of-loop soundings with a short or long offset configuration. The imaging method is based on the same principle as that employed by Fullagerf (1989), with apparent resistivities computed directly from time-derivative data, dh/dt, and then associated with depths according to image theory.

Key words: TEM imaging loop source date apparent resistivity

1 THEORY

1.1 *Central-loop*

The basic formula used in the image method is the TEM response for a central loop configuration over an homogeneous half-space. Ward and Hohmann (1987) give this response as

$$\frac{\partial b_z}{\partial t} = -\frac{I}{\sigma a^3}[3\mathrm{erf}(\theta a) - \frac{2}{\sqrt{\pi}}\theta a(3+\theta^2 a^2)\mathrm{e} - \theta^2 \mathrm{a}^2] \quad (1)$$

where erf$(\theta a)$is the error function

$$\mathrm{erf}(\theta a) = \frac{2}{\sqrt{\pi}}\int_0^{\theta_a} e^{-t^2}\,\mathrm{d}t \quad (2)$$

$$\theta = \sqrt{\mu_0 \sigma/(4t)} \quad (3)$$

and I=source current (A); σ=earth conductivity (s/m); a=radius of transmitter loop (m); μ_0=permeablity of the earth taken to be $4\pi\times10^{-7}$ H/m; t=time (s)

For early times θ is larger

$$\frac{\partial b_z}{\partial t} \approx -\frac{3I}{\sigma a^3} \quad (4)$$

while for late times and small θ

$$\frac{\partial b_z}{\partial t} \approx -\frac{I\sigma^{3/2}\mu_0^{5/2}a^2}{2\sqrt{\pi}}t^{-5/2} \quad (5)$$

1.2 *Apparent Resistivity*

We would like to compute apparent resistivities directly from the time-derivative response $\partial b_z/\partial t$. One useful approach to this problem is to define the apparent resistivity separately for early and late times according to formulas (4) and (5) respectively. However, neither of those two resistivities clearly shows by its shape the properties of the geoelectrical section in the intermediate time range. Another approach to the problem, as described by Spies and Raiche (1980), Raiche and Spies (1981), and Sheng (1986), is to compute an "exact" apparent resistivity directly from equation (1) instead of equations (4) and (5). For computing the "exact" resistivity, we need to solve the equation

①Supported by the National Natural Science Fundation of China and National Science Foundation of USA;
Manuscrigt received Oct. 16, 1992

$$\frac{\partial b_z}{\partial t} - \frac{\partial b_m}{\partial t} = 0 \qquad (6)$$

where $\partial b_z / \partial t$ is based on equation (1) and $\partial b_m / \partial t$ is the measured field at a given time. There are two possible apparent resistivity solutions at each time from equation (6). One of the solutions approaches the early time resistivity at early times, and another one conforms with the late time resistivity at late times. In the general case, the two solutions will have a joint point at an intermediate time such that an "exact" apparent resistivity can be found by combining the two solutions. Fig.1 shows the comparison of the "exact" apparent resistivities and the early times and late times apparent resistivities. The solid and dashed lines represent the two solutions from equation (6), while the curves marked as "· · " and "oo" are the early times and late times apparent resistivities from equations (4) and (5) respectively. The "exact" apparent resistivity can be formed by combining the data before the joint point of one solution and the data after the joint point of another solution. The "exact" apparent resistivity is clearly better than the results computed by the asymptotic formulas. Unfortunately, as Raiche (1983), Spies and Eggers (1986), and Sheng (1986) have pointed out, there still exist some problems in this "exact" computing method. In some particular cases, there is no meaningful definition in the intermediate time range for the "exact" apparent resistivity as shown in Fig.2 (a) and 3 (a). After examining the problems, we found that they have the same feature as the static shift. The fact that equation (1) is linear with respect to an arbitrary multiplicative constant makes it possible to find meaningful definitions for the unmeaningful apparent resistivity curves in the intermediate time range. To make the correction, the measured field data are multiplied by an arbitrary scaling constant determined in the interpretation processing. For example, multiplying a scaling constant which is greater than one makes the divergent solutions in Fig.2 (a) shift together to form a joint point between the two solutions so that a smooth transition can be defined between the two solutions as shown in Fig.2 (b). For the data in Fig.3 (a) the data is multiplied by a constant less than one which shifts the two solutions apart so that the "exact" apparent resistivity in the intermediate time is redefined as shown in Fig.3 (b). This technique is called calibration correction. The calibration correction can yield meaningful definitions for the unmeaningful apparent resistivity in the intermediate times.

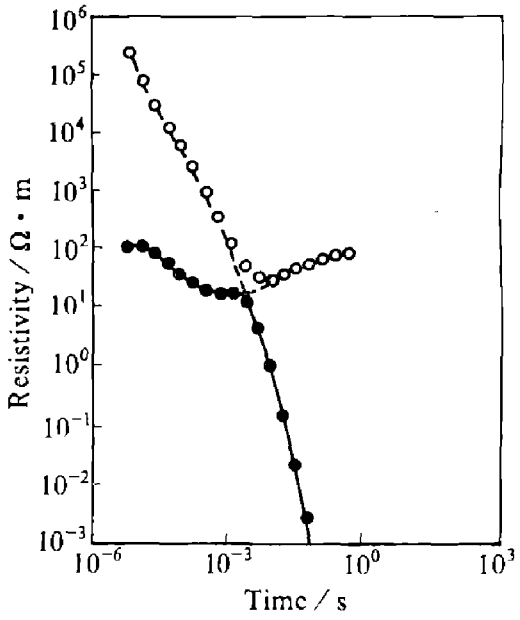

Fig. 1 Comparison of the "exact" apparent resistivity and the early and late time apparent resistivity

Solid and dashed lime—solutions of "exact" appa res;
●—early time appa res; ○—late time appa res

1.3 *Diffusion Depth*

Diffusion depths are computed from diffusion velocity. For the case of an homogeneous ground of conductivity σ, as described by Nekut (1987), the mean field penetration depth can be written as

$$\tilde{h} = \sqrt{2t / (\mu_0 \sigma)} \qquad (7)$$

the time-domain equivalent of the usual skin-depth formula. From equation (7) the mean field

penetration velocity is given by

$$V = \frac{\mathrm{d}\tilde{h}}{\mathrm{d}t} = \frac{1}{\sqrt{2t\mu_0\sigma}} \tag{8}$$

or $$V = \sqrt{\rho / (2t\mu_0)} \tag{9}$$

For given times t_i and t_{i+1}, assume the depth at time t_i is known as h_i, the depth at t_{i+1} is computed by

$$h_{i+1} = h_i + \frac{V_i + V_{i+1}}{2}(t_{i+1} - t_i) \tag{10}$$

where

$$\left.\begin{aligned} V_i &= \sqrt{\rho_i / (2t_i\mu_0)} \\ V_{i+1} &= \sqrt{\rho_{i+1} / (2t_{i+1}\mu_0)} \end{aligned}\right\} \tag{11}$$

and ρ_i and ρ_{i+1} are the apparent resistivities at time t_i and t_{i+1} respectively which are computed from equation (6).

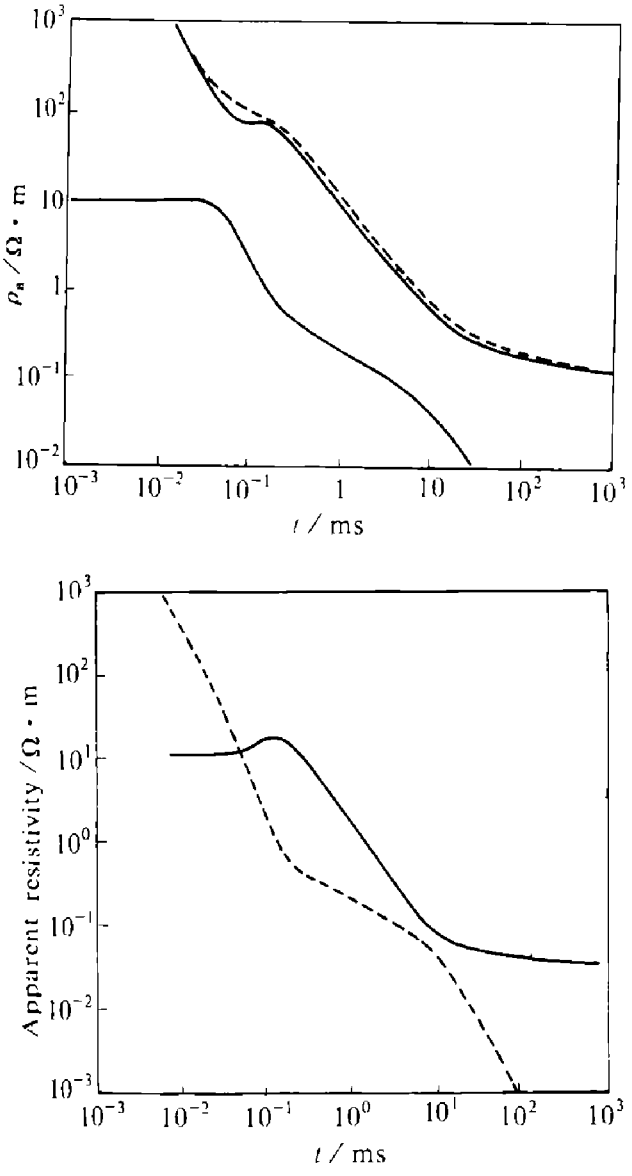

Fig. 2 Calibration correction of the "exact" apparent resistivity.

(a)—Since the curves diverge, no smooth transition exists between the early-time and late-time curves; (b)—After calibration correcting, there is a smooth transition between the early-time and late-time curves

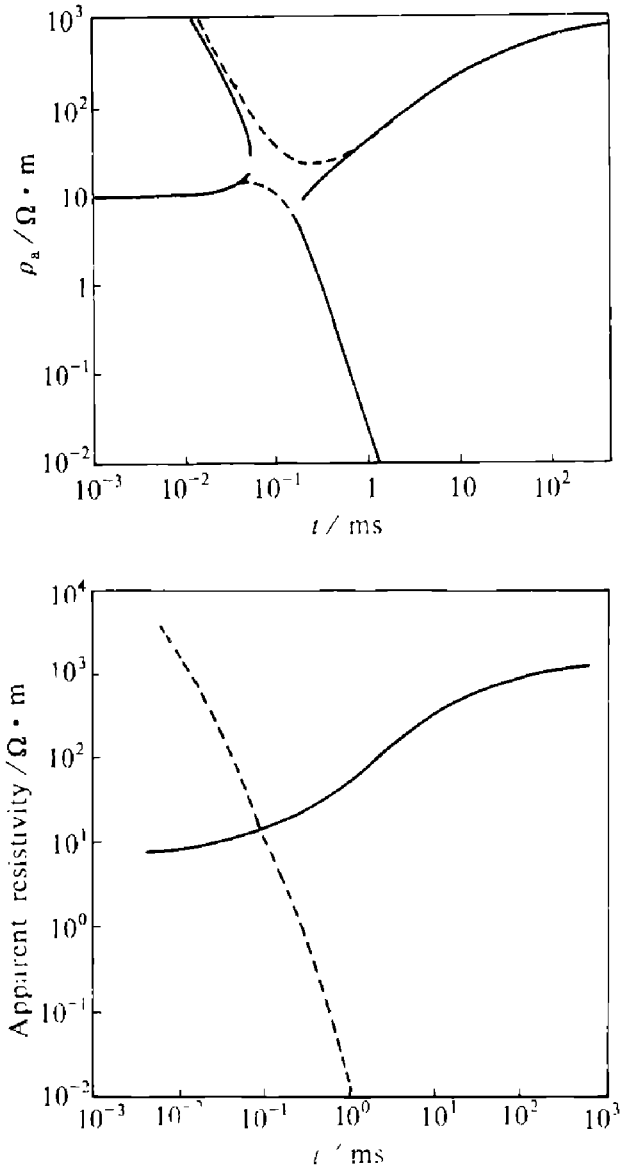

Fig. 3 Calibration correction of "exact" apparent resistivity

(a)—The "exact" apparent resistivity is undefined in the region 0.05 to 0.18 ms; (b)—After calibration correcting, the "exact" apparent resistivity in that region is redefined

1.4 *Alternate Apparent Resistivity Estimate*

Apparent resistivity also can be estimated from the cumulative conductance, which is defined as the integrated total conductance from the surface to a certain depth h. Thus, from the

$$\frac{dt}{dh} = \int_0^h \mu_0 \sigma dh \tag{12}$$

the conductivity can be estimated directly by taking a derivative with respect to the depth h,

$$C_i = \frac{1}{\mu_0} \frac{d^2 t}{dh^2}\Big|_{h=h_i} \tag{13}$$

The apparent resistivity then is defined by

$$\rho_{i,2} = 1 / \sigma_i \tag{14}$$

Since h_i can be obtained from equation (10) and it is known, $\rho_{i,2}$ is easily estimated from equation (14).

Using equations (13) and (14) to estimate resistivity involves taking a second derivative with respect to a dependent variable h which is dependent on the apparent resistivity estimated from equation (6). This operation is therefore unstable when the data contain much noise. It is recommended that the user should be careful when using this parameter as the final interpretation result. If the TEM data are not distorted by much noise, even though variable h is dependent on the aparent resistivity estimated from equation (6), the alternate apparent resistivity $\rho_{i,2}$ is closer to the true resistivity than that apparent resistivity estimated from equation (6).

1.4.1 Non Central Loop

Non-central loop configurations include inside-loop as well as outside-loop configurations. TEM sounding data collected from a non- central loop configuration are inverted by transforming the data to an equivalent central-loop sounding response and interpreting the transformed data by using the central-loop interpretation technique described above. The transformation method is simple, involving only the determination of two parameters from two experimental formulas. The two parameters are functions only of the offset (the distance from the center of the transmitter loop to the receiver position) and the actual transmitter loop size. They are independent of the geoelectric section.

The first parameter determines the loop size of the equivalent central loop configuration. This parameter is only dependent on the actual offset of the non-central loop configuration. The simple experimental formula is

$$a = 1.6 \text{ offset} \tag{15}$$

where a is the side length of the equivalent square central loop configuration

The second parameter, which is a function of the actual loop size and offset, is calculated by multiplying the sounding data. The experimental formula, based on the regression method, is

$$P_2 = P_1 r / (r_1) \tag{16}$$

where P_1 is defined by

$$\lg_{10}(P_1) = 2.04 \lg_{10} (O / r) + 0.42 \tag{17}$$

and

P_2—the parameter used to modify the non central loop sounding data;

O—offset of actual non-central loop configuration;

r—the length of the longer side of the actual transmitter loop;

r_1—the length of the shorter side of the actual transmitter loop

Fig.4 is an example comparing the time-derivative response of a transformed non-central loop configuration with that of the equivalent central-loop configuration. The non-central loop time-derivative response is measured at an offset of 707.1 m ($(x, y) = (500, 500)$) with a 100 m × 100 m transmitter loop.The dashed line is the negative response while the solid line represents the positive response. After multiplying by the second parameter 144.1, obtained from equations (16) and (17), the non-central loop response becomes the curve marked as • and o which coincides with a central loop response with a loo

size 1 131.4 m × 1 131.4 m, consistent with equation (15), except for the data in the area of the sign change which are eliminated automatically in the program. Hence, the non-central loop time-derivative response can be inverted by imaging the transformed data (i.e. the raw data multiplied by a parameter obtained from equations (16) and (17)) as a central loop data with the changed loop-size [from equation (15)].

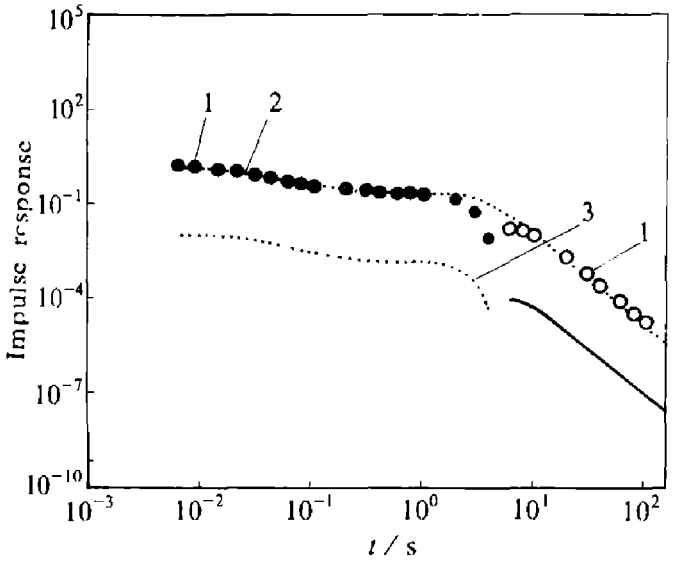

Fig. 4 Comparison of transformed long-offset data and equivalent central-loop data

1—Transformed long-offset response;
2—Central loop response; 3—long offset response

1.4.2 Grounded Source

TEM sounding data collected from a grounded line source configuration are also interpreted by transforming the response to an equivalent central-loop sounding and imaging the transformed response by using the central-loop interpretation technique described above. For a grounded source configuration, the homogeneous half-space voltage response can be expressed as (Stoyer *et al.* 1983),

$$v(t,t_0)=\frac{AIL\sin\varphi}{2\pi r^4\sigma}\left[3\mathrm{erf}(u)-\frac{2}{\sqrt{\pi}}u(3+2u^2)e^{-u^2}\right] \quad (18)$$

where

$$u=\sqrt{t_0/t}=r\sqrt{\mu_0\sigma/4t}$$

and

A—effective area of the receiver (m^2);

I—source current(A);

L—length of source wire(m);

r—source-receiver distance (m);

σ— the homogeneous earth conductivity (s / m);

μ_0—permeability of the earth taken to be $4\pi \times 10^{-7}$ H / m;

t—time (s);

φ—angle between the source dipole and r (distance) (°);

$t_0=\mu_0 r^2\sigma/4$ is the characteristic time (Tikhonov, 1946)

Comparing equation (18) with equation (1), we see that the two equations are equivalent except for the scale constant

$$c=2\pi r/AL\sin\varphi \quad (19)$$

Thus after multiplying by the scale constant c given in equation (19), the voltage response in equation (18) is equivalent to the time-derivative response of a central-loop configuration with a loop radius r.

2 EXAMPLES

2.1 *Layered Earth*

In Fig.5, two-layer model results are presented. TEM time-derivative responses were computed for two models at delay times ranging from 6 μs to 800 ms for a 200 m × 200 m loop. The origin of the coordinate of the system is located at the center of the loop. In Fig.5 (a), the true resistivity abruptly increases by a factor of 10 at depth 400 m. In Fig.5 (b), it abruptly decreases by a factor of 10 at the same depth. Receiver (0, 0) is for a central-loop configuration, while receiver (0, 500) is for a long offset configuration. Both interpreted results approximate the true electric variation with the depth beneath each sounding station.

In Fig.6, three-layer model results are presented. As in the case of the two-layer models,

central-loop and non-central loop responses were computed for the three-layer model at delay time ranging from 6 μs to 100 ms with a 100 m × 100 m transmitter loop. All of the inversion results indicate the resistivity characteristics of the true model. Note that when the true resistivity decreases with depth the estimated resistivity shows an overshoot and when the true resistivity increases with depth the estimated resistivity changes much slower to the higher resistivity than the true resistivity changes. These problems should be kept in mind to avoid interpretation mistakes.

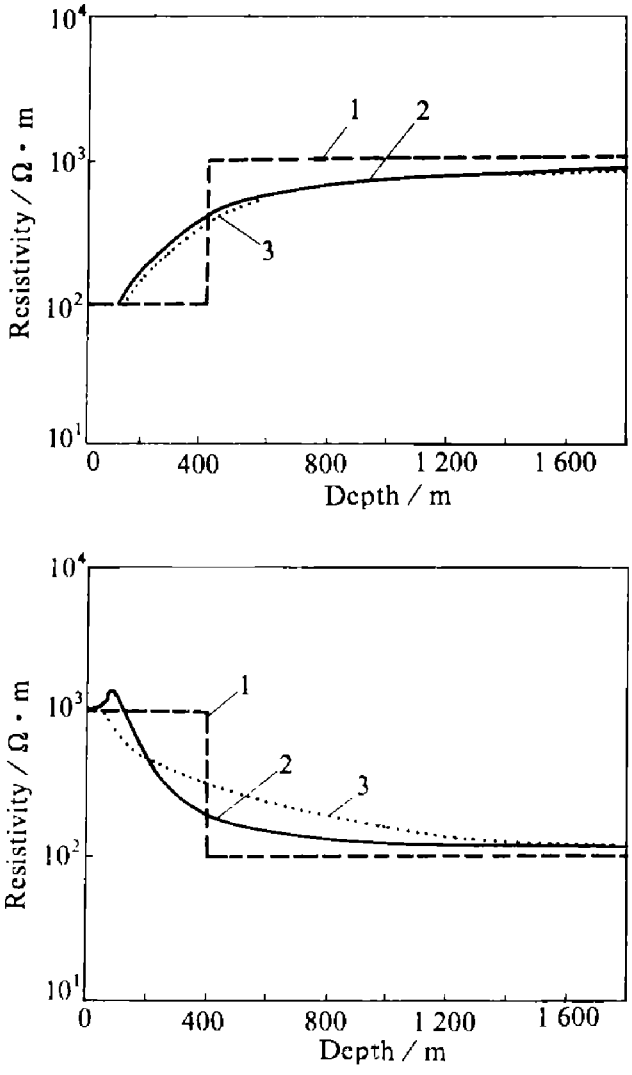

Fig. 5 Two-layer earth models inversion results

1—True model; 2—Receiver (0,0); 3—Receiver (0,500)

2.1.1 3-D Model

A 3-D model electromagnetic response suite was computed for experiments to determine the optimal use of the imaging algorithm when a 3-D structure is present. The 3-D model is a 200 m wide × 200 m long × 100 m thick 10 Ω-m conductor in a 500 Ω-m half-space. The source is a 100 m × 100 m transmitter loop. The first test is the inversion of multi-receiver data along the $x=0$ axis from one transmitter loop. Fig.7 illustrates the case of a profile measurement for a transmitter loop centered at position (0, 0, 0). The inversion results are symmetric with respect to the 3-D body since the measurement configuration is symmetric. From this resistivity cross section, one can confirm there is a conductive 3-D body under the surface, although its resistivity is not accurately determined.

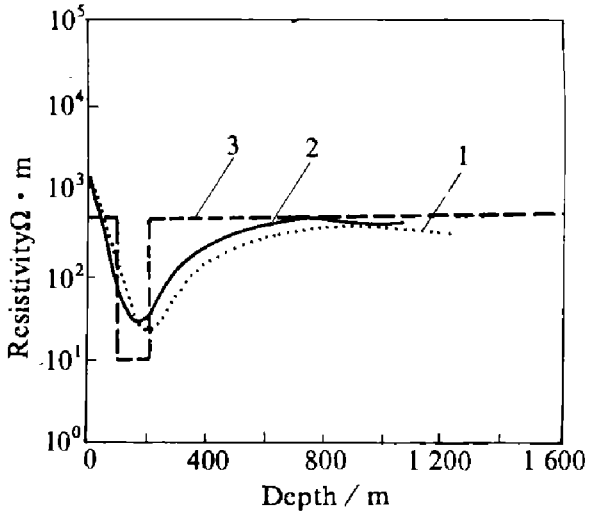

Fig. 6 Three-layer earth model inversion result

1—Receiver (0,100); 2—Receiver (0,0); 3—True model

Fig.8 shows a resistivity cross-section from the image program for a model which is the same as in Fig.7 except that the transmitter loop is centered at position $x=-200$. This cross-section is much more complex than the last one since the configuration is not symmetric with respect to the 3-D body. From this cross-section, the interpreter can suspect a shallow 3-D body under the surface but cann't confirm its position. Furthermore, the higher resistivity anomaly beyond the 3-D body can lead to misinterpretation accord-

ing to this cross-section.

Is the higher resistivity anomaly in fact caused by the imaging technique? To determine whether this was true, we examined the responses of another model. A layered earth cross-section response suite was computed with the same

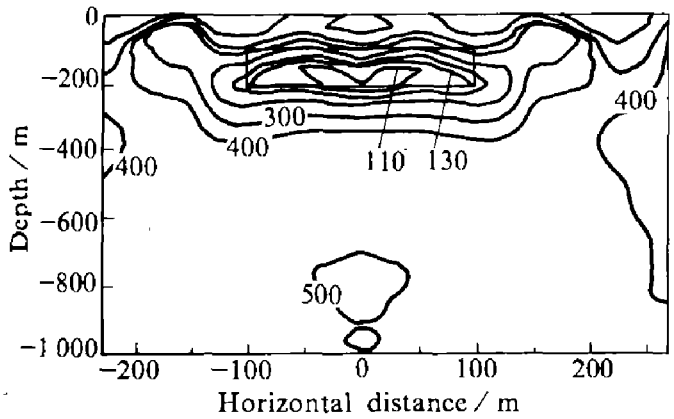

Fig. 7 Inversion resistivity cross-section

(Transmitter loop is centered at position 0)

configuration as that in Fig.8. The resistivities of the layered earth are $\rho_1 = 500$ Ωm, $\rho_2 = 10$ Ωm, and $\rho_3 = 500$ Ωm, while the thicknesses of the layers are $h_1 = 100$ m and $h_2 = 100$ m. The 100 m × 100 m transmitter loop is centered at position −200 m, and the TEM responses at several receivers along the profile were calculated. The inversion results shown in Fig.9 indicate a layered earth structure under the surface. Even though there is still a higher resistivity anomaly near the surface between positions 0 and 200, the anomaly is much lower and much shallower than the 3−D body case when the second layer becomes limited. As a result, it can be concluded that the higher resistivity anomaly beyond the 3−D body is mainly caused by the 3−D body when an asymmetric configuration and a 1−D interpretation technique are used to detect the 3−D body.

To avoid the misinterpretation of the 3−D structure when a 1−D interpretation program is used, a central-loop or short-offset configuration is recommended. Fig.10 shows a central- loop cross-section. In this case, seven transmitter loops were used for the profile measurements. The seven loops were centered at −300 m, −200 m, −100 m, 0 m, 100 m, 200 m, and 300 m respectively. For every transmitter loop only one TEM response was measured at the center of the loop. The inversion results clearly define a 3−D structure under the surface.

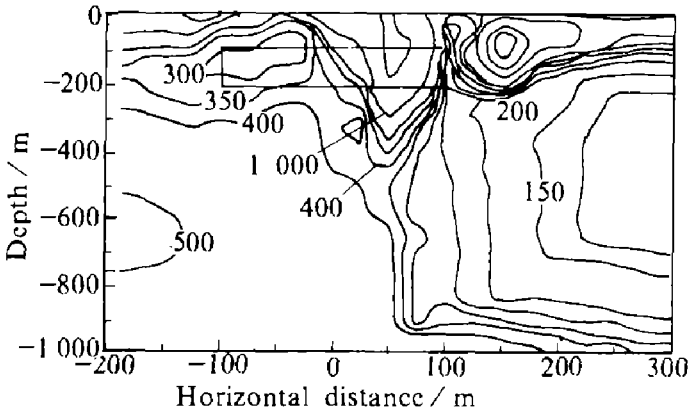

Fig. 8 Inversion resistivity cross-section

(Transmitter loop is centered at position−200)

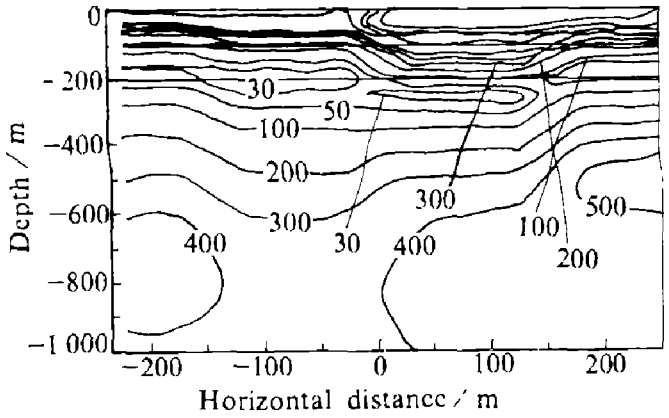

Fig. 9 Layered earth inversion results

(Transmitter loop is centered at position−200)

Fig.10 is a short-offset inversion result. In this case, three transmitter loops (fewer than in the central-loop case) were used to measure the TEM responses. The three loops were centered at −200 m, 100 m, and 300 m respectively. The TEM responses at receiver positions −300 m, −200 m, and −100 m were measured by using transmitter loop 1 (−200 m). Loop 2 (100 m) is used for receivers at 0 m, 100 m, and 200 m, while the last receiver position at 300 m was measured for central-loop configuration loop 3.

The inversion results are compatable with the central-loop results (Fig.11). This configuration is more efficient than the central-loop configuration in collecting data in field work.

One problem arising from the image interpretation method is that the interpreted depth is deeper than the actual depth. This is caused by the diffusion velocity of the image current in an inhomogeneous circumstance. The estimated depth can be modified by a scaling factor to confirm the actual depth.

Another problem for this technique in interpreting 3—D structure is that it can not reach the true resistivity. Even the 3—D body in a 500 Ω—m half-space has a 10 Ω—m in the 3—D structure example described above (Fig.10 and 11), the estimated resistivity can only reach 100 Ω—m due to the larger contrast in the resistivities of the 3—D body and the homogeneous half-space. Comparing with the layered earth inversion results (Fig.9), it is found that the undershoot of the estimated resistivity probably results from the 3—D body dimensions. A larger 3—D body leads to better resistivity resolution.

2.1.2 Grounded Source Example (LOTEM)

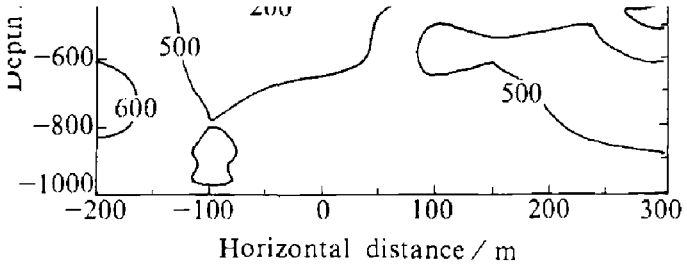

Fig. 10 Short-offset configuration inversion results

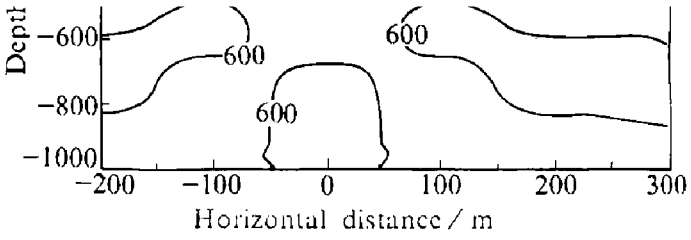

Fig. 11 Central-loop configuration inversion resutls

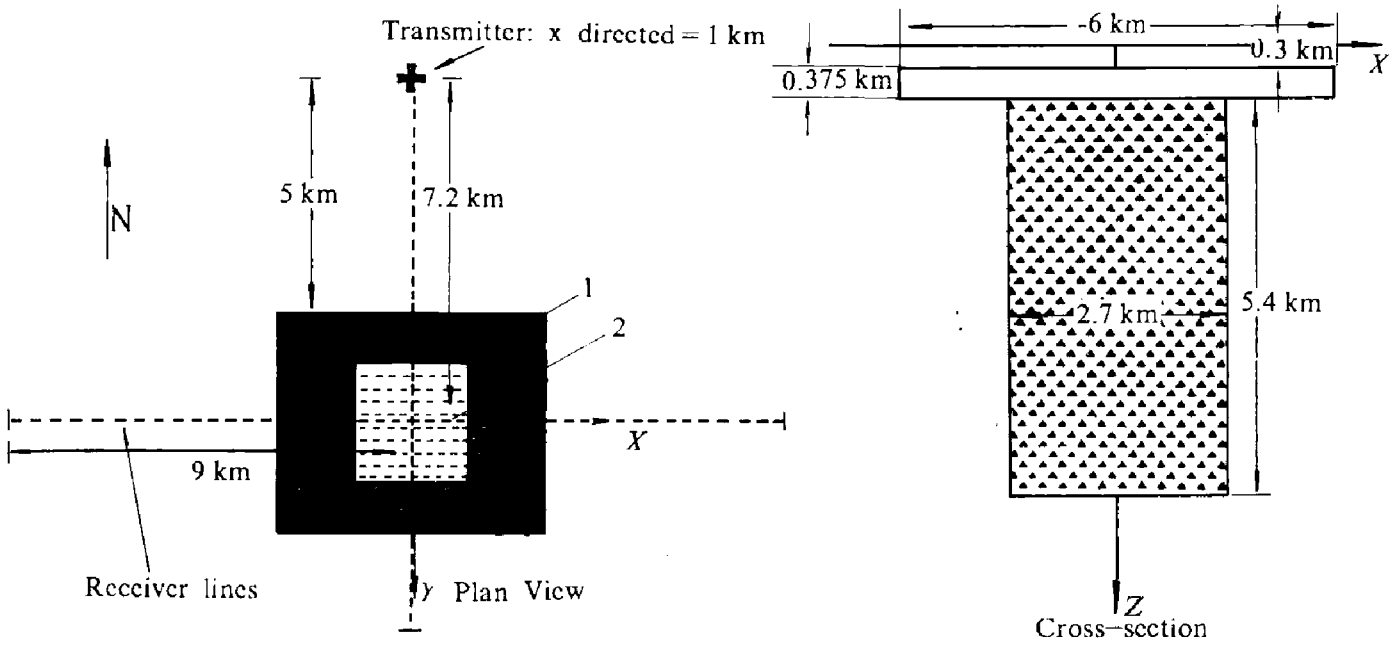

Fig. 12 Geothermal synthetic model

1—Clay cap 5 Ω · m. Host 200 Ω · m 2—Reservoir Model 1—25 Ω · m

The grounded source example is a synthetic geothermal model. The model geometry, shown in Fig.12 (a) and (b), consists of a 5 Ω−m clay cap over a geothermal reservoir of resistivity 25 Ω−m in a 200 Ω−m half-space. The 1 km long transmitting source is 7.2 km away from the center of the 3−D body (see Fig.12 (b)). Synthetic data were computed by Louise Pellerin with her EM3D program. The estimated resistivity cross-section shown in Fig.13 computed from the image program clearly defines the clay cap and the geothermal reservoir which is superimposed on the cross-section.

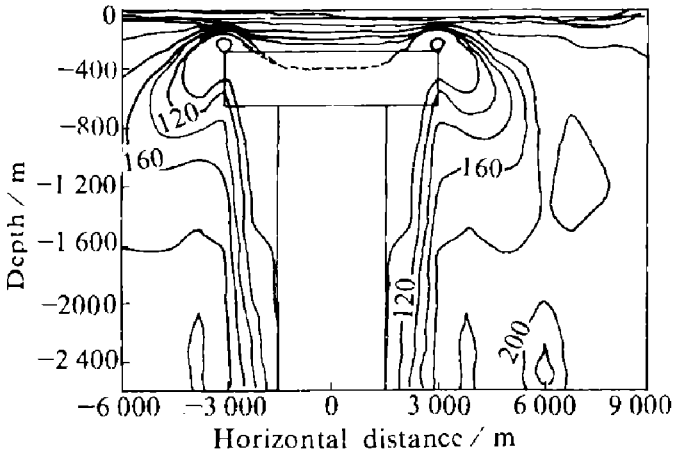

Fig. 13 Grounded source configuration inversion results

3 CONCLUSIONS AND RECOMMENDATIONS

From the examples described above, it can be concluded that this image program can approximately interpret TEM data including ungrounded loop source and grounded line source soundings. Loop source data can be the responses of central-loop soundings or out-of-loop soundings with short or long-offset configurations. For detecting 3−D structures with a loop source configuration, it is recommended that central-loop or short-offset configurations be used to avoid misinterpretation. The inversion results of the grounded source configuration are not disturbed too much by offset and are better than the results of the long-offset loop source configurations. The reason is that the grounded source response is "exactly" equivalent by a scaling factor to the central-loop source response, while the response of a long-offset loop source is "experimentally" equivalent to a central-loop response.

REFERENCES

1 Eaton, P A; Hohmann, G W. Physics of the Earth and Planetary Interiors, 1989. 53, 384−404.
2 Fullager, P K. Exploration Geophysics, 1989, 1, 43−45.
3 Nekut, A G. Geophysics, 1987, 52: 1431− 1435.
4 Raiche, A P. Geophysics, 1983, 48: 787−789.
5 Raiche, A P; Spies, B R. Geophysics, 1981, 46: 53−64.
6 Sheng, Y. Geophysics, 1986, 51: 1291−1297.
7 Spies, B R; Eggers, D E. Geophysics, 1986, 51: 1462−1471.
8 Spies, B R; Raiche, A P. Geophysics, 1980, 45: 1197−1204.
9 Ward S; Hohmann G.W. In: Electromagnetic Methods in Applied Geophysics, (ed) Nabighian M. N., Society of Exploration Geophysicists, 1985.